

Article

A Modified Polynomial Expansion Algorithm for Solving the Steady-State Allen-Cahn Equation for Heat Transfer in Thin Films

Chih-Wen Chang ^{1,*} , Chein-Hung Liu ¹ and Cheng-Chi Wang ^{2,*}

¹ Department of Mechanical Engineering, National Chung Hsing University, Taichung 40227, Taiwan; carus@dragon.nchu.edu.tw

² Graduate Institute of Precision Manufacturing, National Chin-Yi University of Technology, Taichung 41170, Taiwan

* Correspondence: chihwen.chang8@gmail.com (C.-W.C.); wcc@ncut.edu.tw (C.-C.W.); Tel.: +886-4-2284-0433 (C.-W.C.); +886-4-2392-4505 (ext. 5163) (C.-C.W.)

Received: 20 April 2018; Accepted: 13 June 2018; Published: 15 June 2018



Featured Application: The specific application of the work is for heat and mass transfer.

Abstract: Meshfree algorithms offer a convenient way of solving nonlinear steady-state problems in arbitrary plane areas surrounded by complicated boundary shapes. The simplest of these is the polynomial expansion approach. However, it is rarely utilized as a primary tool for this purpose because of its rather ill-conditioned behavior. A well behaved polynomial expansion algorithm is presented in this paper which can be more effectively used to solve the steady-state Allen-Cahn (AC) equation for heat transfer in thin films. In this method, modified polynomial expansion was used to cope with each iteration of the steady-state Allen-Cahn equation to produce nonlinear algebraic equations where multiple scales are automatically determined by the collocation points. These scales can largely decrease the condition number of the coefficient matrix in each nonlinear system, so that the iteration process converges very quickly. The numerical solutions were found to be accurate and stable against moderate noise to better than 7.5%. Computational results verified the method and showed the steady-state Allen-Cahn equation for heat transfer in thin films could easily be resolved for several arbitrary plane domains.

Keywords: steady-state Allen-Cahn equation; meshless approach; modified polynomial expansion; boundary value problems; heat transfer in thin films

1. Introduction

Much interest has been shown in the solution of the Allen-Cahn (AC) equation, the primary purpose of which has been depiction of the motion of antiphase boundaries in crystalline solids and phase separation in binary alloys [1]. This equation is now utilized in many moving boundary issues involving thermodynamic driving forces in microstructure evolution, domain evolution in thin films, image processing, fluid dynamics, and materials science through a phase-field approach [2–7]. The Allen-Cahn equation has been employed to model diverse phenomena in nature, for example, Beneš et al. [8] proposed a method of pattern recovery (image segmentation) based on solution of the AC equation. The method is often realized as a regularization of the level-set motion by mean curvature where a particular forcing term is added that allows the initial level set to nearly encompass the pattern in question. This demonstrates convergence of the numerical approach and display function of the method for several artificial and real instances.

Feng and Prohl [9] constructed some useful a priori error estimates for proposed numerical schemes. In addition, the optimal order and quasi-optimal order error bounds were displayed for semi-discrete and fully discrete schemes under different constraints of mesh and time step size and with different regularity assumptions about the initial datum function. Later, Wheeler et al. [10] identified three stages of temporal evolution for AC equations: the first corresponds to interfacial genesis, which happens very fast; the second is interfacial motion controlled by diffusion and the local energy difference across the interface; the time scale of the last stage was longer and here curvature effects were pivotal. After this, Sabir et al. [11] employed the mathematical formulation of tumor hypoxia-targeting by presenting the decay parameter of oxygen in a model [12,13]. For numerical calculation the conforming Q1 finite element scheme for space discretization, as well as the second-order diagonally implicit fractional step θ -method for temporal discretization, were used. Note that the distribution of nutrients in tissues has substantial influence on tumor structure and growth rate. Later, Zahra [14] developed a numerical solution based on the nonpolynomial B-spline (trigonometric B-spline) collocation method for solving the AC equation. This algorithm combined the trigonometric B-spline interpolant and the θ -weighted scheme for space and time discretization. Von Neumann stability analysis showed the proposed technique to be unconditionally stable. Bulent et al. [15] investigated the numerical solution of the AC equation with constant and degenerate mobility, as well as with polynomial and logarithmic energy functionals. They discretized the model equation using the symmetric interior penalty Galerkin method in space, and by the average vector field (AVF) method in time. They also showed that the energy stable AVF method as the time integrator for gradient systems, like the AC equation, satisfies the energy decreasing property for a fully discrete scheme. They found that the discrete energy decreased monotonically, phase separation and metastability phenomena could be observed, and the ripening time was detected correctly. After that, Yang et al. [16] addressed the uniform bounds associated with the AC equation and its numerical discretization schemes. These uniform bounds were different from, and weaker than, the conventional energy dissipation and the maximum principle. However, they can be helpful in the analysis of the numerical approach. Moreover, fully discretized schemes on the basis of the Fourier collocation method for spatial discretization and the Strang splitting method for time discretization also preserved the uniform L^2 -bound unconditionally. In all the references above discussions were about time-dependent AC equations and regular domains. There was no mention of time-independent AC equations and irregular domains.

Liu and Kuo [17] used a single-scale and multiple Pascal triangle formulation to cope with linear elliptic partial differential equations (PDEs) in a simply connected domain that has a complicated boundary shape and obtained accurate results. After that, Liu and Young [18] employed a multiple-scale Pascal polynomial to deal with two-dimensional Stokes and inverse Cauchy-Stokes problems and also got good results. Later, Chang [19] addressed steady-state nonlinear heat conduction problems in an arbitrary plane domain enclosed by a complex boundary utilizing a multiple-scale polynomial expansion scheme. In addition, Chang et al. [20] also applied multiple-scale polynomial expansion to tackle the steady-state modified Burgers' equation in transport problems and got good results.

The rest of this paper is organized as follows: Section 2 displays the steady-state Allen-Cahn (AC) equation and a modified polynomial expansion scheme. The multiple-scale idea for the Pascal triangle expansion algorithm, which is totally resolved by the collocation points. The iterative process for solving steady-state AC equations is presented in Section 3. In Section 4, numerical examples for these issues are given. Section 5 offers some concluding remarks.

2. The Steady-State Allen-Cahn Equation and a Modified Polynomial Expansion Method

We start with the steady-state Allen-Cahn equation as follows:

$$\Delta u(x, y) = u - u^3 + H(x, y), (x, y) \in \Omega, \quad (1)$$

$$u(x, y) = G(x, y), (x, y) \in \Gamma_1, \quad (2)$$

$$u_n(x, y) = F(x, y), (x, y) \in \Gamma_2, \tag{3}$$

where Δ is the Laplacian operator, and F, G and H are given functions. Γ is the boundary of issue domain Ω with $\Gamma = \Gamma_1 \cup \Gamma_2$, and n is a unit outward normal on Γ . Under the presented Dirichlet boundary condition (2) and the Neumann boundary condition (3), we can resolve Equation (1) to acquire a solution of $u(x, y)$.

Then, we employ the polynomial expansion as a trial solution of the PDE and formulate the needed algebraic equations after a suitable collocation in the problem area. However, this is rarely utilized as a major numerical tool to resolve the nonlinear PDEs. The main reason being that the resultant nonlinear algebraic equations (NAEs) are often seriously ill-conditioned.

The elements in the polynomial matrix are as follows:

$$\begin{bmatrix} 1 & y & y^2 & \dots & y^{m-1} & y^m \\ x & xy & xy^2 & \dots & xy^{m-1} & xy^m \\ x^2 & x^2y & x^2y^2 & \dots & x^2y^{m-1} & x^2y^m \\ \vdots & \vdots & \vdots & \dots & \vdots & \vdots \\ x^m & x^m y & x^m y^2 & \dots & x^m y^{m-1} & x^m y^m \end{bmatrix} \tag{4}$$

are often utilized to expand the solution of $u(x, y)$. If the elements are restrained from the upper-left triangle, the result is the famous Pascal triangle expansion:

$$\begin{array}{cccccccc} & & & & 1 & & & & \\ & & & & x & y & & & \\ & & & x^2 & xy & y^2 & & & \\ & & x^3 & x^2y & xy^2 & y^3 & & & \\ & x^4 & x^3y & x^2y^2 & xy^3 & y^4 & & & \\ & x^5 & x^4y & x^3y^2 & x^2y^3 & xy^4 & y^5 & & \\ \dots & \end{array} \tag{5}$$

Consequently, the solution $u(x, y)$ is expanded by

$$u(x, y) = \sum_{i=1}^m \sum_{j=1}^i p_{ij} x^{i-j} y^{j-1}, \tag{6}$$

where the coefficients p_{ij} are to be resolved, where the number of all elements is $n = m(m + 1)/2$. The highest order of the above polynomial is $m - 1$.

From Equation (6), the following equations can be directly stated:

$$u_x(x, y) = \sum_{i=1}^m \sum_{j=1}^i p_{ij} (i - j) x^{i-j-1} y^{j-1}, \tag{7}$$

$$u_y(x, y) = \sum_{i=1}^m \sum_{j=1}^i p_{ij} (j - 1) x^{i-j} y^{j-2}, \tag{8}$$

$$u_n \Big|_{(x,y) \in \Gamma} = \sum_{i=1}^m \sum_{j=1}^i p_{ij} [(i - j) x^{i-j-1} y^{j-1} n_x + (j - 1) x^{i-j} y^{j-2} n_y], \tag{9}$$

$$\Delta u(x, y) = \sum_{i=1}^m \sum_{j=1}^i p_{ij} [(i - j)(i - j - 1) x^{i-j-2} y^{j-1} + (j - 1)(j - 2) x^{i-j} y^{j-3}]. \tag{10}$$

Introducing these equations to Equations (1)–(3), and selecting n_1 and n_2 collocation points on the boundary and in the area, to satisfy the boundary condition and the field equation, we obtain a system of NAEs to deal with the n coefficients p_{ij} .

The multi-scale Pascal triangle is then introduced as follows. Because x and y in the issue area Ω may be arbitrarily large, the above expansion would lead to a divergence of the powers x^m and y^m . To acquire an accurate solution of an AC equation employing the modified Pascal triangle polynomial expansion scheme, we have to develop a more accurate and effective method to cope with these NAEs by reducing the condition numbers. A new multiple-scale Pascal triangle is obtained by expansion of $u(x,y)$ by

$$u(x,y) = \sum_{i=1}^m \sum_{j=1}^i p_{ij} s_{ij} x^{i-j} y^{j-1}, \tag{11}$$

in which the scales s_{ij} are decided as below.

The coefficients p_{ij} utilized in the expansion (6) can be demonstrated as an n -dimensional vector \mathbf{p} with components $p_k, k = 1, \dots, n$ by

$$\begin{aligned} &k = 0 \\ &\text{Do } i = 1, m \\ &\text{Do } j = 1, i \\ &k = k + 1 \\ &p_k = p_{ij} \\ &\text{Enddo.} \end{aligned} \tag{12}$$

After that, for a generic point $(x,y) \in \bar{\Omega}$, the term $u(x,y)$ can be displayed as an inner product of a vector \mathbf{a} with \mathbf{p} , i.e.,

$$u(x,y) = [1 \quad x \quad y \quad x^2 \quad xy \quad y^2 \quad x^3 \quad x^2y \quad xy^2 \quad y^3 \quad \dots] \begin{bmatrix} p_1 \\ p_2 \\ p_3 \\ \vdots \\ p_n \end{bmatrix} = \mathbf{a}^T \mathbf{p}. \tag{13}$$

Likewise, for a generic point $(x,y) \in \Omega$, the term $\Delta u(x,y)$ can be displayed as an inner product of a vector \mathbf{q} with \mathbf{p} , in which the components q_k are of the type $q_k = (i-j)(i-j-1)x^{i-j-2}y^{j-1} + (j-1)(j-2)x^{i-j}y^{j-3}$.

Then, while we select n_1 points $(x_i, y_i), i = 1, \dots, n_1$ on the boundary Γ to satisfy the boundary condition, and n_2 points $(x_i, y_i), i = 1, \dots, n_2$ on the area Ω to satisfy the field equation. For example, for Laplace's equation we have

$$\mathbf{A} = \begin{bmatrix} \mathbf{a}_1^T \\ \vdots \\ \mathbf{a}_{n_1}^T \\ \mathbf{q}_1^T \\ \vdots \\ \mathbf{q}_{n_2}^T \end{bmatrix}, \mathbf{b} = \begin{bmatrix} G(x_1, y_1) \\ \vdots \\ G(x_{n_1}, y_{n_1}) \\ 0 \\ \vdots \\ 0 \end{bmatrix}. \tag{14}$$

We can cope with a normal linear system in place of $\mathbf{A}\mathbf{p} = \mathbf{b}$:

$$\mathbf{K}\mathbf{p} = \mathbf{b}_1 \tag{15}$$

where

$$\begin{aligned} \mathbf{b}_1 &= \mathbf{A}^T \mathbf{b}, \\ \mathbf{K} &= \mathbf{A}^T \mathbf{A} > 0. \end{aligned} \tag{16}$$

The conjugate gradient method (CGM) can be employed to resolve Equation (15).

If we investigate the norm of each column of the coefficient matrix of \mathbf{A} is equal, the multiple-scale s_{ij} is equal to $\|\mathbf{p}_1\| / \|\mathbf{p}_k\|$, where $s_{11} = 1$ and \mathbf{p}_k denotes the k th column of \mathbf{A} in Equation (16). Such that in the new system

$$\mathbf{I}\mathbf{p} = \mathbf{b}, \tag{17}$$

the n column norms of the new coefficient matrix \mathbf{B} are equal.

Let $M_k = s_{ij}$, and we can present a post conditioning matrix:

$$\mathbf{Q} := \text{diag}(M_1, \dots, M_n), \tag{18}$$

such that the above equilibrated multiple-scale skill is equivalent to acquiring the new coefficient \mathbf{I} by

$$\mathbf{I} = \mathbf{A}\mathbf{Q}. \tag{19}$$

3. The Iterative Process for the Steady-State Allen-Cahn Equation

At the start, we utilize $p_{ij} = p_{ij}^0$ and (u, u_x, u_y) are calculated by

$$u(x, y) = \sum_{i=1}^m \sum_{j=1}^i p_{ij} s_{ij} x^{i-j} y^{j-1}, \tag{20}$$

$$u_x(x, y) = \sum_{i=1}^m \sum_{j=1}^i p_{ij} (i-j) s_{ij} x^{i-j-1} y^{j-1}, \tag{21}$$

$$u_y(x, y) = \sum_{i=1}^m \sum_{j=1}^i p_{ij} (j-1) s_{ij} x^{i-j} y^{j-2}, \tag{22}$$

After that, upon collocating n_k points to satisfy the boundary conditions (2) and (3) and the field equation $\mathbf{A}\mathbf{p} = \mathbf{b}$, we can formulate a coefficient matrix \mathbf{A} from the left-hand side of the field equation with the aid of Equations (7)–(10), and then by employing the multiple-scale s_{ij} , therefore \mathbf{P} via Equation (18). Meanwhile a tentative right-hand side \mathbf{b}_0 is acquired from the right-hand side of Equation (1) by introducing Equations (20)–(22). Hence, we have a linear system with a different right-hand side:

$$\mathbf{A}\mathbf{Q}\mathbf{p} = \mathbf{b}_k, \tag{23}$$

whose normal form is handled by the CGM to generate a new coefficient p_{ij}^1 . Iteration is continued until convergence.

The numerical processes this algorithm uses to resolve the steady-state AC equation are outlined in the following steps.

- (i) Given n_1, n_2 ($n_k = n_1 \times n_2$), and m [$n = m(m+1)/2$].
- (ii) Given p_{ij}^0 .
- (iii) Given collocation points $(x_i, y_i), i = 1, \dots, n_k$.
- (iv) One-time only:

Generate $s_{ij}, s_{ij} = \|\mathbf{p}_1\| / \|\mathbf{p}_k\|,$

Generate \mathbf{Q} from $M_k = s_{ij}$ and Equation (18),

$$\mathbf{I} = \mathbf{A}\mathbf{Q}. \tag{24}$$

- (v) For $k = 0, 1, 2, \dots$, reiteration as follows:

Compute u, u_x, u_y from Equations (20)–(22)

Generate \mathbf{b}_k from the right-hand side of Equation (1)

Resolve the normal form of $\mathbf{I}\mathbf{p} = \mathbf{b}_k$ to acquire

$$p_{ij}^{k+1} \tag{25}$$

If p_{ij}^k converges in accordance with a given stopping criterion $\sqrt{\sum_{i=1}^m \sum_{j=1}^i (p_{ij}^{k+1} - p_{ij}^k)^2} < \varepsilon_2$, which is a named relative distance coefficient, then stop; otherwise, go to step (iv).

4. Numerical Examples

4.1. Example 1

We first consider the following AC equation in heat transfer of thin films in an arbitrary domain (peanut shape, Cassini shape, gear shape, and amoeba-like irregular shape) as shown in Figure 1.

$$\Delta u = u - u^3 + H(x, y), \tag{26}$$

$$\rho(\theta) = 0.3\sqrt{\cos(2\theta) + \sqrt{1.1 - \sin^2(2\theta)}}, \tag{27}$$

$$\rho(\theta) = \left[\cos 4\theta + \sqrt{18/5 - \sin^2 4\theta} \right]^{1/3}, \tag{28}$$

$$x = 0.5[2 + 0.5 \sin(7\theta)] \cos[\theta + 0.5 \sin(7\theta)], y = 0.5[2 + 0.5 \sin(7\theta)] \sin[\theta + 0.5 \sin(7\theta)], \tag{29}$$

$$\rho(\theta) = \exp[\sin(\theta)] \sin^2(2\theta) + \exp[\cos(\theta)] \cos^2(2\theta), \tag{30}$$

where ρ is the radius function of Γ , $H(x, y) = u^3 - u + 6\exp(xy^3 + x^3y) - 6x^2y(x^2 + 2y^2)$ and the closed-form solution is

$$u = x^3y^3(\exp -x). \tag{31}$$

Under the Dirichlet boundary condition, for the peanut domain, with $n_1 = 27, n_2 = 4 (n_k = 108), m = 7$, and $n = 28$, we employed the multiple-scale expansion method by using the CGM under the convergence criterion $\varepsilon_1 = 10^{-8}$. At $\varepsilon_2 = 10^{-8}$, the iterative process reaches convergence after 7 iterations and the results are shown in Figure 2a,b. The numerical error is shown in Figure 3, the maximum error being 1.88×10^{-10} . For the Cassini-shaped domain, with $n_1 = 26, n_2 = 2 (n_k = 52), m = 8, n = 36$, and a convergence criterion of $\varepsilon_1 = 10^{-12}$. At $\varepsilon_2 = 10^{-12}$, the iterative process reaches convergence after 11 iterations and the results are shown in Figure 4a,b. The numerical error is plotted in Figure 5, the maximum error being 1.40×10^{-13} . For the gear irregular domain, under $n_1 = 25, n_2 = 2 (n_k = 50)$, the same m, n , and convergence criterion $\varepsilon_1 = 10^{-3}$. At $\varepsilon_2 = 10^{-3}$, convergence is reached after 8 iterations and the results are shown in Figure 6a,b. The numerical error is plotted in Figure 7, the maximum error being 3.09. Comparison with the maximum absolute value of 124.88 of $u(x, y)$, shows this error to be acceptable. For the amoeba-like irregular domain, with $n_1 = 50, n_2 = 2 (n_k = 100)$, the same m, n , and convergence criterion, convergence is reached after 11 iterations and the results are shown in Figure 8a,b. The numerical error is plotted in Figure 9 and the maximum error is 9.04×10^{-9} . Note that the multiple-scale method is highly efficient, and it can provide a very accurate solution. Furthermore, to the authors' best knowledge, there are no existing published reports of numerical solutions to this problem that provide more accurate results than these.

To address concern about the stability of this scheme when boundary data were perturbed by random noise, an investigation was carried out with random noise added to the boundary data. For the amoeba-like irregular domain, with $n_1 = 60, n_2 = 2 (n_k = 120), m = 8, n = 36$, and convergence criterion $\varepsilon_1 = 10^{-4}$. At $\varepsilon_2 = 10^{-4}$, convergence was reached after 100 iterations and the results are shown in Figure 10a,b. The numerical error plot is shown in Figure 11 and the maximum error was 0.36. Note that the multiple-scale method still gives an accurate result with imposed noise equal to 0.5.

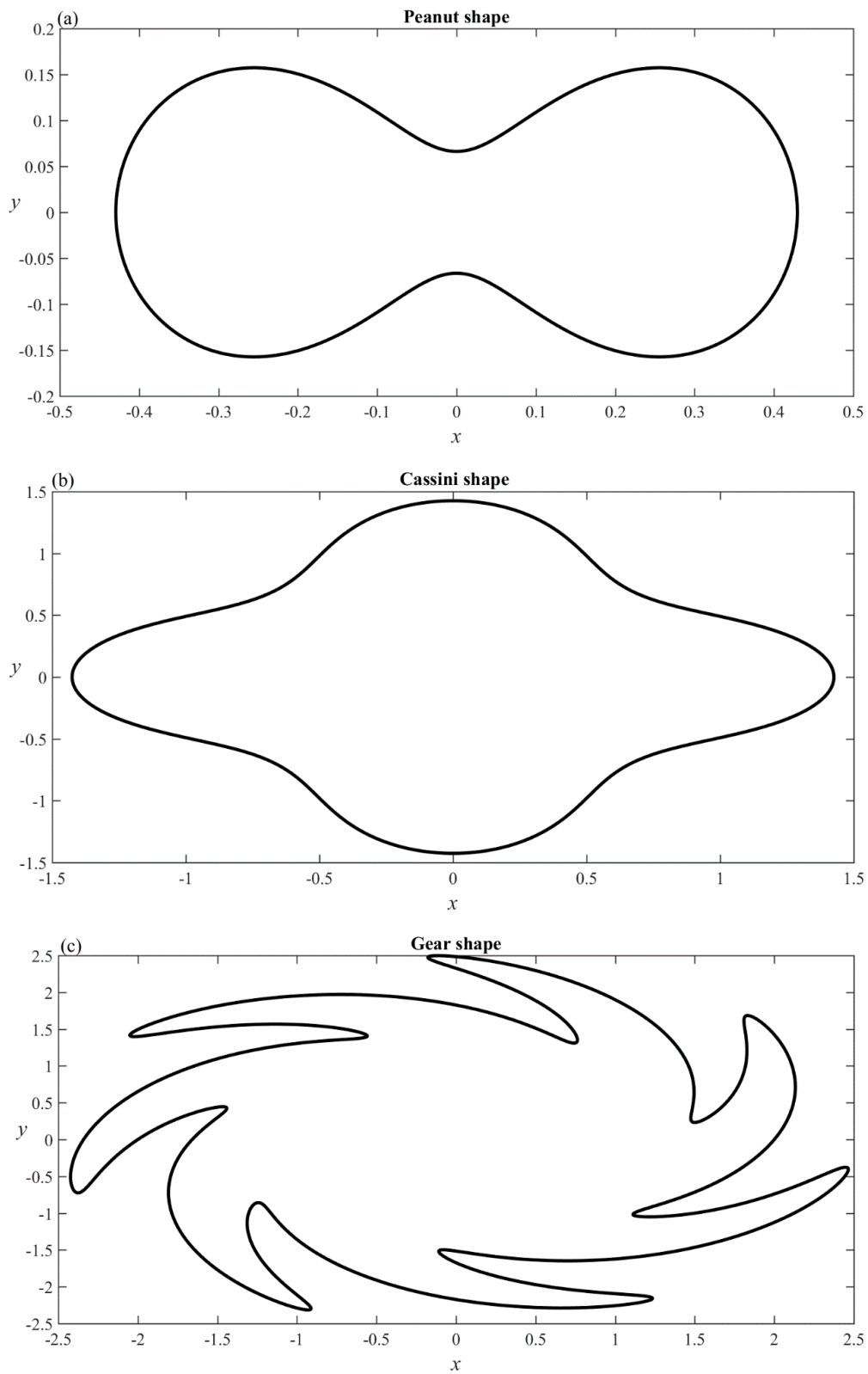


Figure 1. Cont.

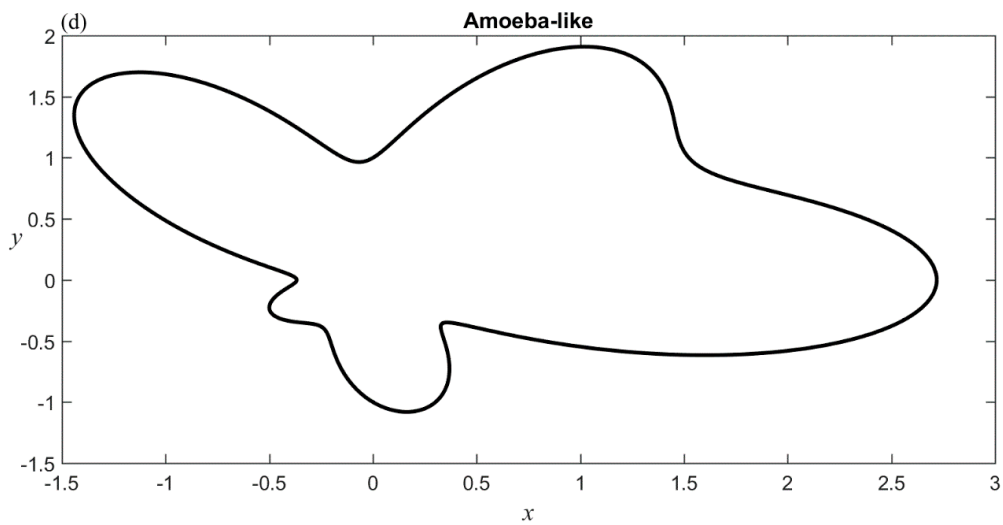


Figure 1. Four geometric configurations of the Allen-Cahn (AC) equation in heat transfer of thin films are shown in (a) the peanut shape, in (b) the Cassini shape, in (c) the gear irregular shape, and in (d) the amoeba-like irregular shape.

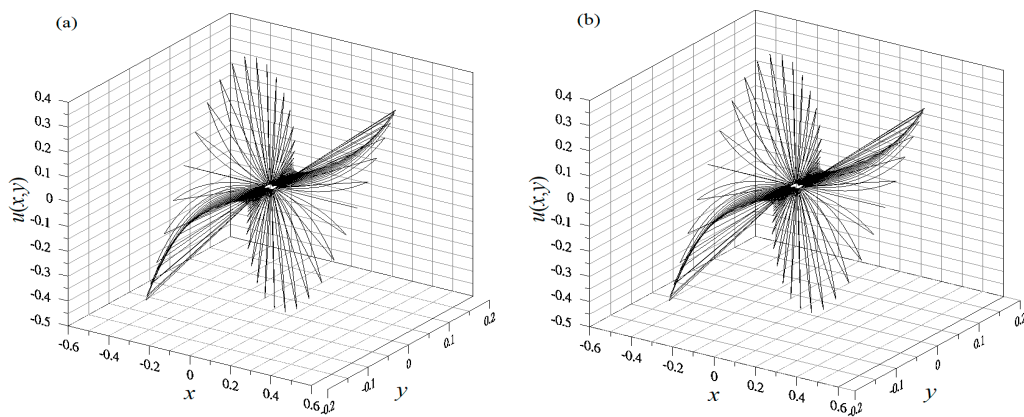


Figure 2. The exact solutions for the steady-state AC equation with peanut-shaped domain are shown in (a), and in (b) the proposed approach solution without random noise.

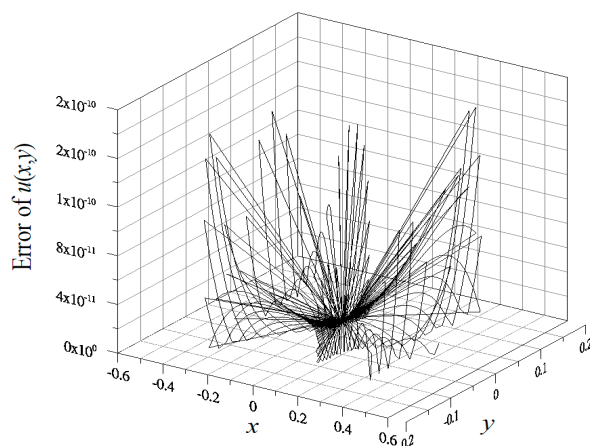


Figure 3. The numerical errors of the proposed solution method for the steady-state AC equation with peanut-shaped domain.

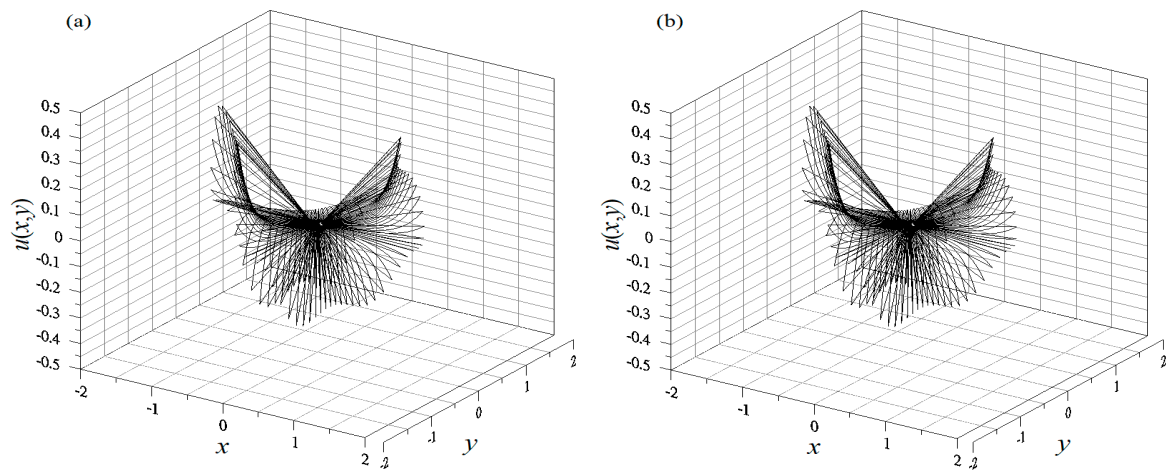


Figure 4. The exact solutions for the steady-state AC equation with Cassini-shaped domain are shown in (a), and in (b) the proposed approach solution without random noise.

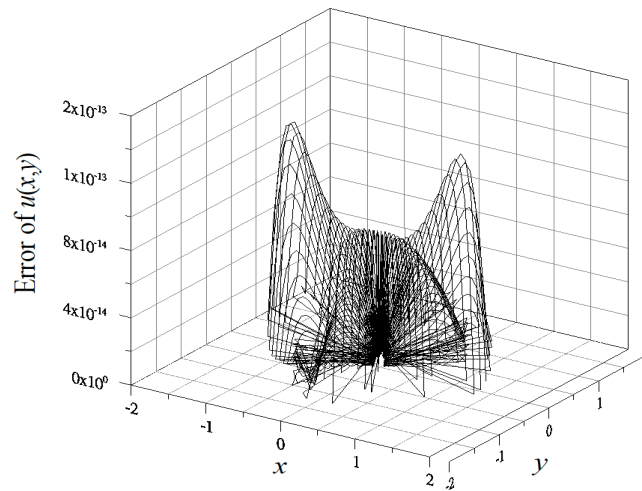


Figure 5. The numerical errors of the proposed method solution for the steady-state AC equation with Cassini-shaped domain.

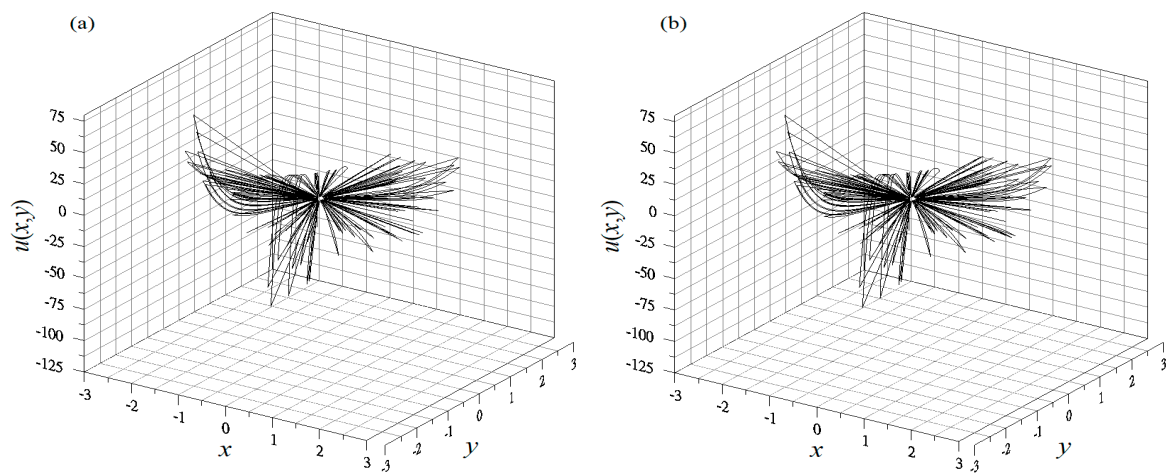


Figure 6. The exact solutions for the steady-state AC equation with gear irregular domain are shown in (a), and in (b) the proposed approach solution without random noise.

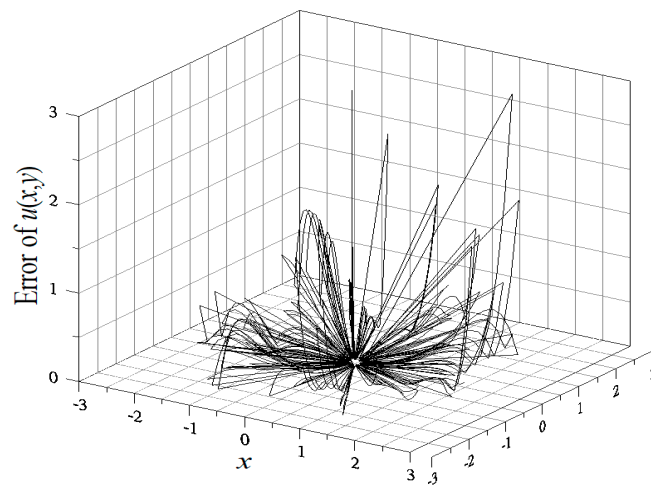


Figure 7. The numerical errors of the proposed method solution for the steady-state AC equation with gear irregular domain.

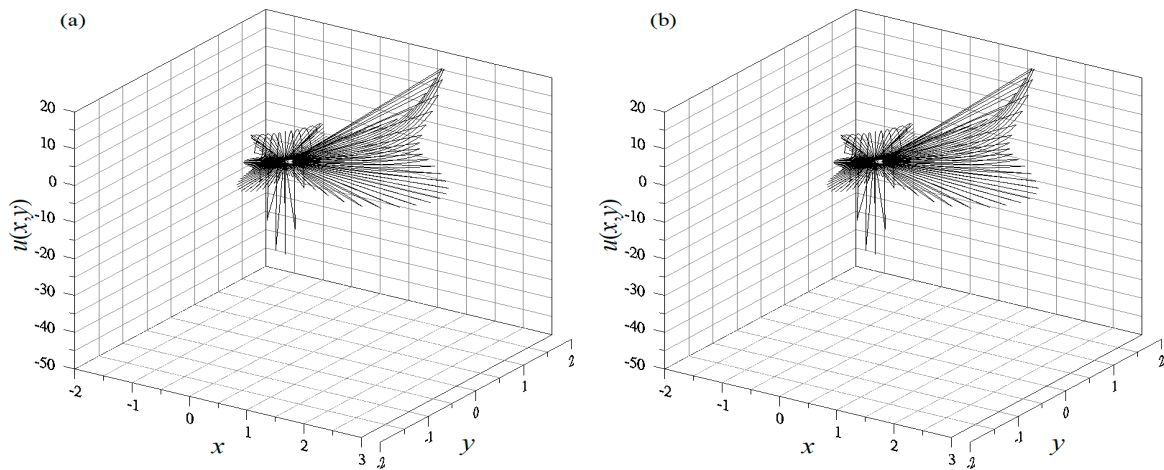


Figure 8. The exact solutions for the steady-state AC equation with amoeba-like irregular domain are shown in (a), and in (b) the proposed approach solution without random noise.

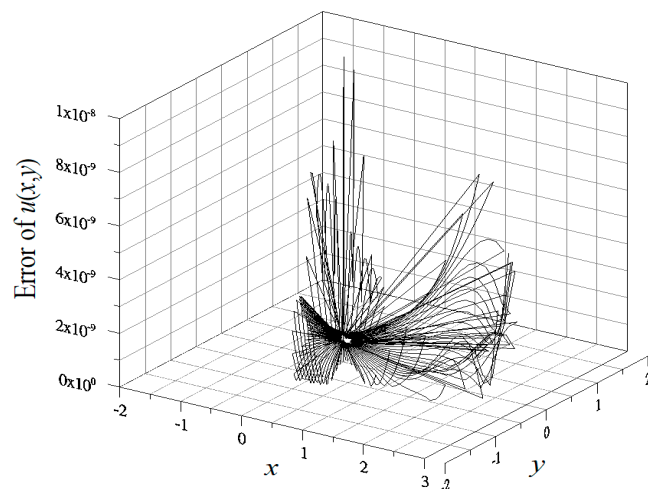


Figure 9. The numerical errors of the proposed method solution for the steady-state AC equation with amoeba-like irregular domain.

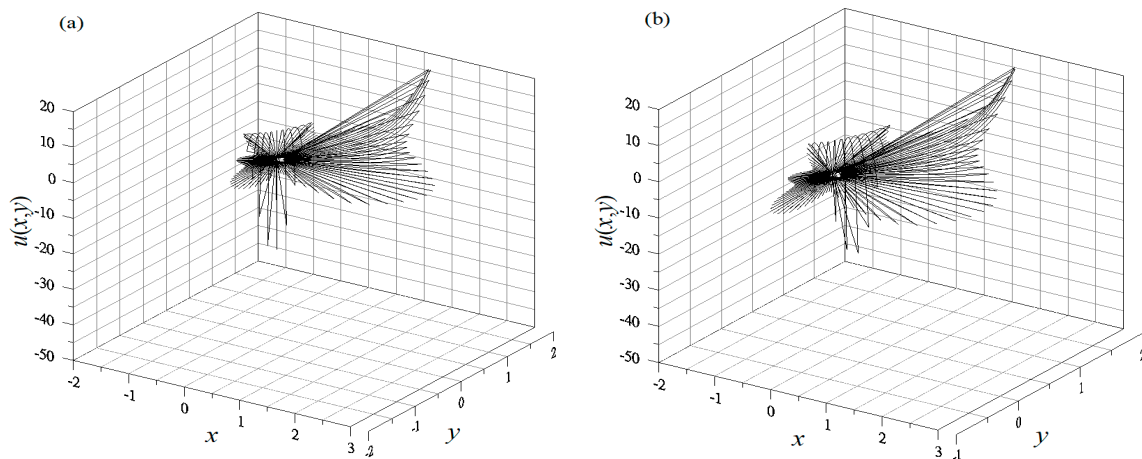


Figure 10. The numerical solutions for the steady-state AC equation with amoeba-like irregular domain are shown in (a), and in (b) the proposed approach solution with random noise.

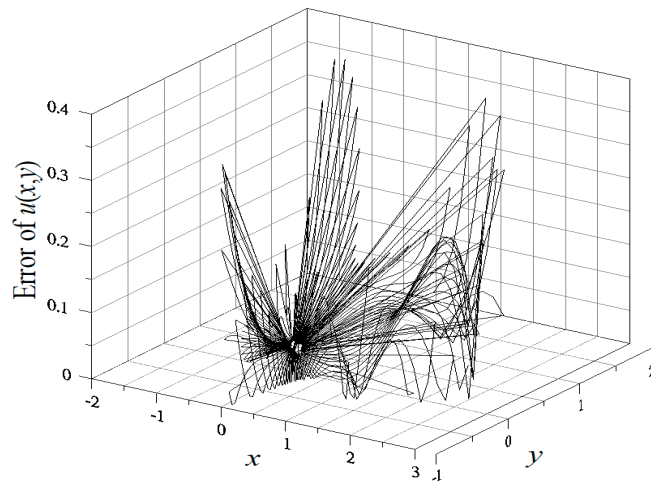


Figure 11. The numerical errors with random noise.

4.2. Example 2

A steady-state AC equation was derived for these four shape domains, where $H(x,y) = u^3 - 3\exp \cdot \sin(x)\sin(y)$ and the closed-form solution is:

$$u = \exp \cdot \sin(x) \sin(y). \tag{32}$$

Under the Dirichlet boundary condition, for the peanut domain, with $n_1 = 28, n_2 = 4 (n_k = 112), m = 7,$ and $n = 28,$ a multiple-scale expansion approach was utilized by applying the CGM with a convergence criterion of $\epsilon_1 = 10^{-11}$. At $\epsilon_2 = 10^{-11}$, convergence was reached after 6 iterations and the results are shown in Figure 12a,b. The numerical error is shown in Figure 13, the maximum error being 5.82×10^{-9} . For the Cassini-shaped domain, with $n_1 = 50, n_2 = 10 (n_k = 500), m = 12, n = 78,$ and convergence criterion of $\epsilon_1 = 10^{-10}$. At $\epsilon_2 = 10^{-10}$, convergence was reached after 17 iterations and the results are shown in Figure 14a,b. The numerical error is shown in Figure 15, and the maximum error was 2.45×10^{-9} . For the irregular gear domain, with $n_1 = 65, n_2 = 3 (n_k = 195), m = 5, n = 15,$ and convergence criterion of $\epsilon_1 = 10^{-2}$. At $\epsilon_2 = 10^{-2}$, convergence was reached after 15 iterations and the results are shown in Figure 16a,b. The numerical error is shown in Figure 17, and the maximum error was 0.61. Comparison with the maximum absolute value of 2.71 of $u(x, y)$ shows the above error to be acceptable. For the amoeba-like irregular domain, with $n_1 = 50, n_2 = 2 (n_k = 100), m = 11, n = 66,$

and convergence criterion of $\varepsilon_1 = 10^{-7}$. At $\varepsilon_2 = 10^{-7}$, convergence was reached after more than 100 iterations and the results are shown in Figure 18a,b. The numerical error is shown in Figure 19, and the maximum error was 1.70×10^{-3} . Note that the multiple-scale scheme is highly efficient, and it can offer a very accurate solution. To the authors' best knowledge, there are no existing published reports of numerical solutions to this problem that provide more accurate results than these.

Concern about the stability of this scheme, where the boundary data were perturbed by random noise, was investigated by adding random noise to the boundary data. For the amoeba-like irregular domain, with $n_1 = 35$, $n_2 = 2$ ($n_k = 70$), $m = 7$, $n = 28$, and convergence criterion of $\varepsilon_1 = 10^{-2}$. At $\varepsilon_2 = 10^{-2}$, convergence was reached after more than 100 iterations and the results are shown in Figure 20a,b. The numerical error is shown Figure 21, and the maximum error was 0.23. Note that the multiple-scale method can acquire accurate results with imposed noise as large as 7.5%.

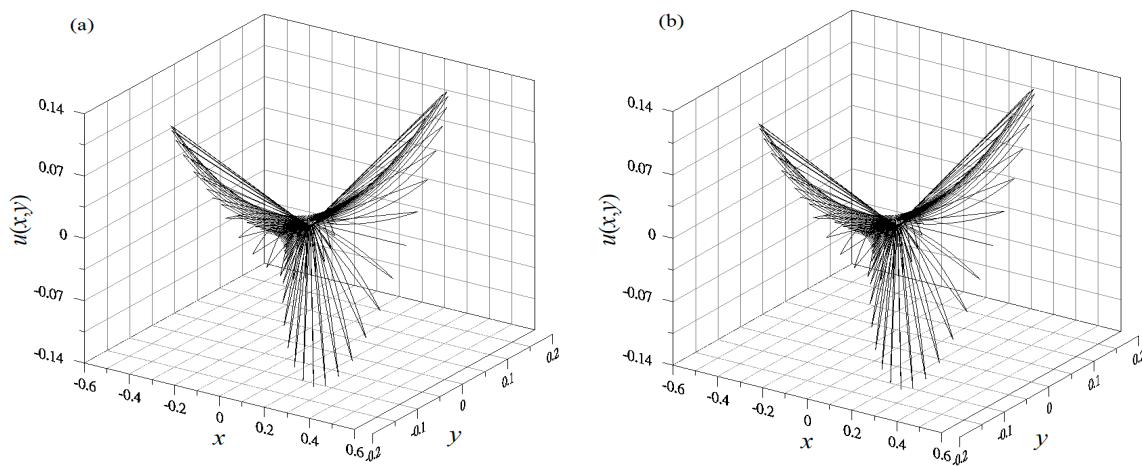


Figure 12. The exact solutions for the steady-state AC equation with peanut-shaped domain are shown in (a), and in (b) the proposed approach solution without random noise.

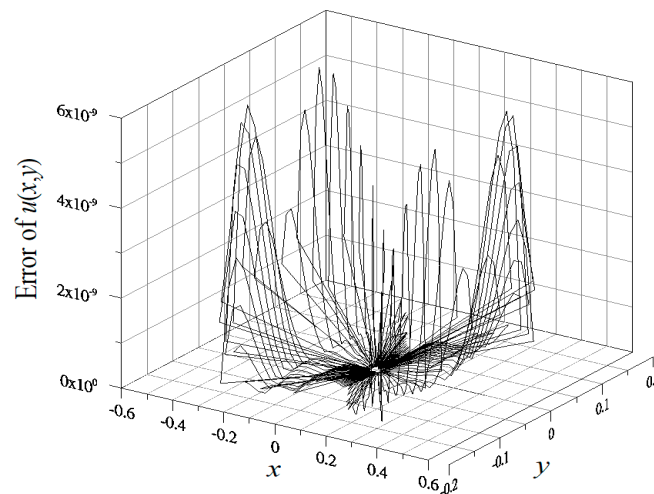


Figure 13. The numerical errors of proposed method solution for the steady-state AC equation with a peanut-shaped domain.

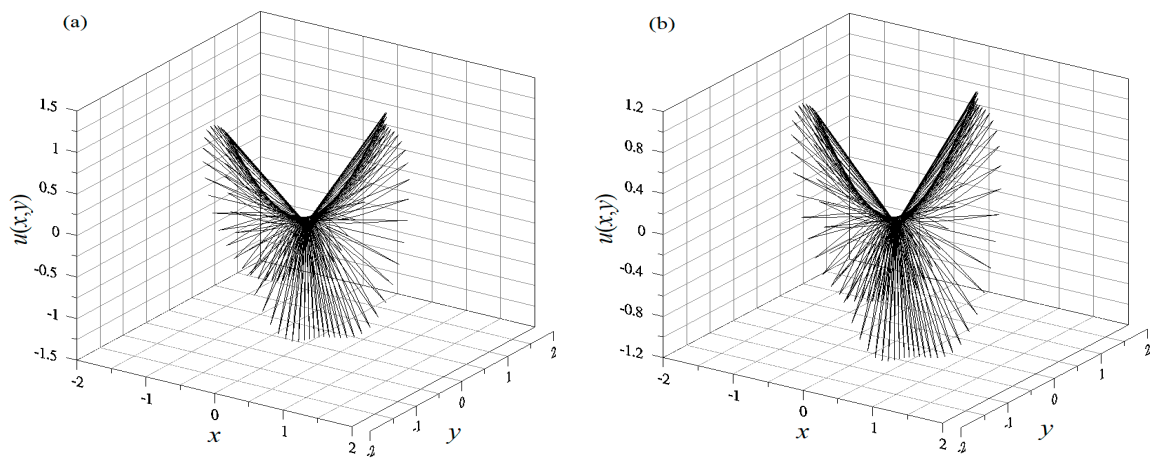


Figure 14. The exact solutions for the steady-state AC equation with Cassini-shaped domain are shown in (a), and in (b) the proposed approach solution without random noise.

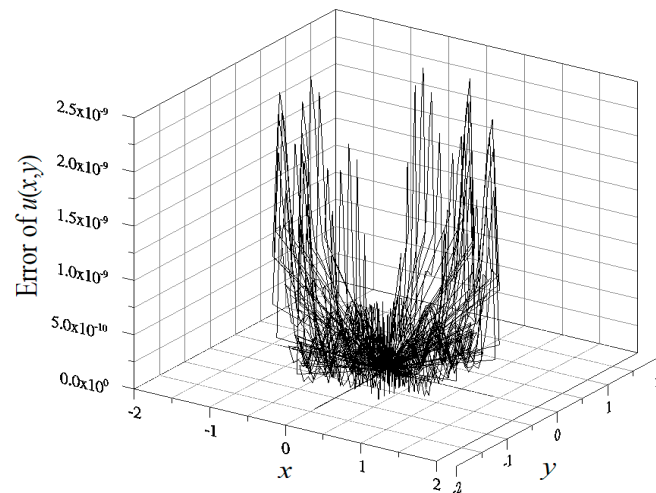


Figure 15. The numerical errors of proposed approach solution for the steady-state AC equation with a Cassini-shaped domain.

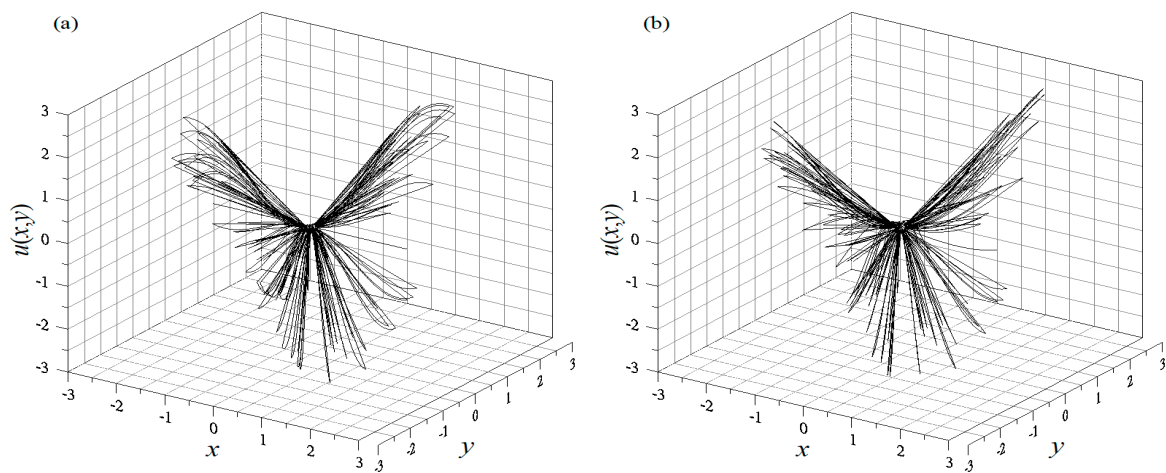


Figure 16. The exact solutions for the steady-state AC equation with irregular gear shaped domain are displayed in (a), and in (b) the proposed approach solution without random noise.

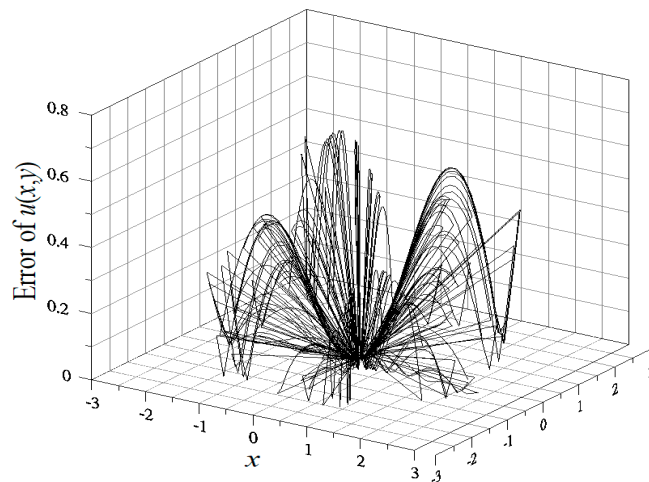


Figure 17. The numerical errors of the proposed method solution for the steady-state AC equation with the gear shaped irregular domain.

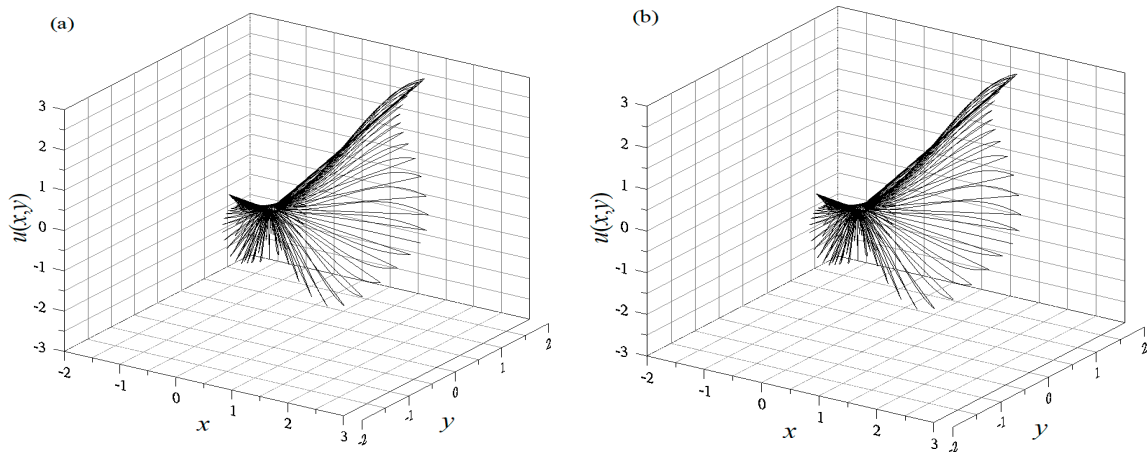


Figure 18. The exact solutions for the steady-state AC equation with amoeba-like irregular domain are shown in (a), and in (b) the proposed scheme solution without random noise.

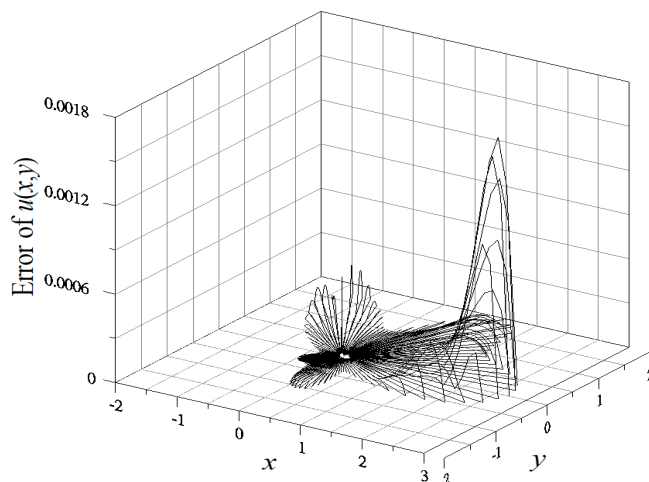


Figure 19. The numerical errors of the proposed method solution for the steady-state AC equation with the amoeba-like irregular domain.

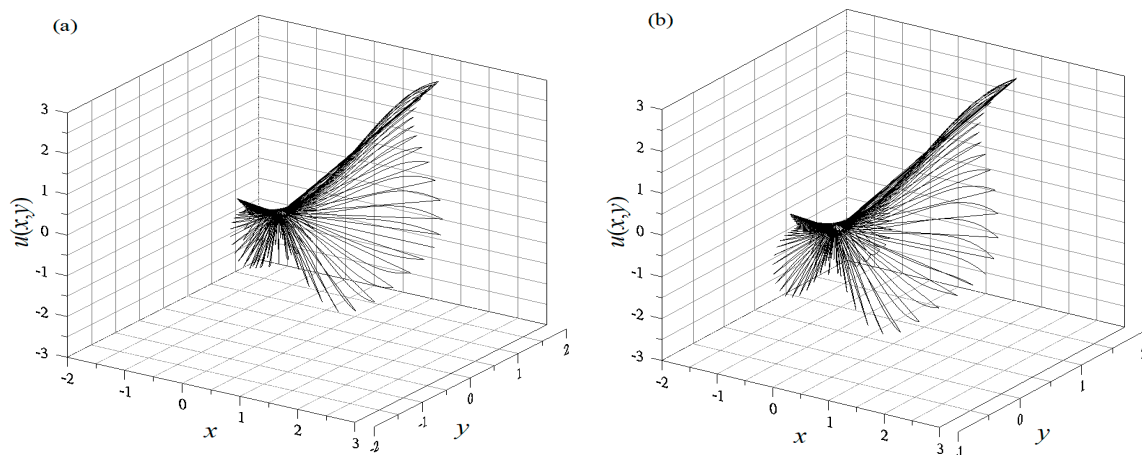


Figure 20. The numerical solutions for the steady-state AC equation with amoeba-like irregular domain are shown in (a), and in (b) the proposed approach solution with random noise.

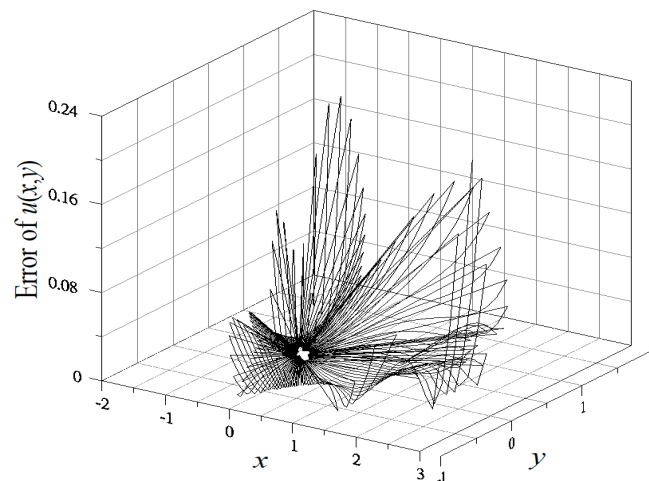


Figure 21. Numerical errors with random noise.

5. Conclusions

In this study a new meshless algorithm was developed to solve steady-state Allen-Cahn equations for heat transfer in thin films with several arbitrary plane domains. In the modified polynomial expansion algorithm proposed, we were able to make decisions about better values of s_{ij} based on the idea of an equilibrated matrix to acquire a multiple-scale s_{ij} in a closed-form which was completely determined by the collocation points. We found that the presented approach is applicable to two-dimensional steady-state Allen-Cahn equations and based on the numerical examples, computationally very efficient, even with large amounts of random noise (up to 7.5%) in the amoeba-like irregular domain. The maximum numerical errors of our scheme are in the order of $O(10^{-1})$ with the amoeba-like irregular domain. The current algorithm can be extended to deal with the three-dimensional and complex steady-state nonlinear PDEs, fourth-order nonlinear steady-state PDEs and many other practical engineering issues.

Author Contributions: C.-W.C. designed and performed the numerical experiments and analyzed the data. C.-W.C., C.-H.L. and C.-C.W. wrote the paper.

Funding: This research was funded by Ministry of Science and Technology of the Republic of China under grants MOST 107-2634-F-005-001, MOST 107-2823-8-005-002, MOST-106-3114-8-005-003, MOST-106-2221-E-167-012-MY2 and MOST-106-2622-E-167-010-CC3.

Acknowledgments: The authors would like to express their deepest appreciations to three anonymous reviewers, who provided constructive comments on the paper.

Conflicts of Interest: The authors declare no conflict of interest.

References

- Allen, M.; Cahn, J.W. A microscopic theory for antiphase boundary motion and its application to antiphase domain coarsening. *Acta Metall. Mater.* **1979**, *27*, 1085–1095. [[CrossRef](#)]
- Shah, A.; Sabir, M.; Bastain, M.P. An efficient time-stepping scheme for numerical simulation of dendritic crystal growth. *Eur. J. Comput. Mech.* **2017**, *25*, 475–488. [[CrossRef](#)]
- Gerish, A.; Moelans, A.; Blanpain, B.; Wollants, P. An introduction to phase-field modeling of microstructure evolution. *Calphad* **2008**, *32*, 268–294.
- Rizwan, M.; Shah, A.; Yuan, L. A central compact scheme for numerical solution of two phase incompressible flow using Allen-Cahn phase-field model. *J. Braz. Soc. Mech. Sci. Eng.* **2016**, *38*, 433–441. [[CrossRef](#)]
- Chen, L.-Q. Phase-field models for microstructure evolution. *Annu. Rev. Mater. Res.* **2002**, *32*, 113–140. [[CrossRef](#)]
- Biben, T. Phase-field models for free-boundary problems. *Eur. J. Phys.* **2005**, *26*, 47–55. [[CrossRef](#)]
- Jay, D.; Lee, B.-J. Effect of constriction on phonon transport in silicon thin films and nanowires. *Smart Sci.* **2016**, *4*, 173–179.
- Beneš, M.; Chalupecky, V.; Mikula, K. Geometrical image segmentation by the Allen-Cahn equation. *Appl. Numer. Math.* **2004**, *51*, 187–205. [[CrossRef](#)]
- Feng, X.B.; Prohl, A. Numerical analysis of the Allen-Cahn equation and approximation for mean curvature flows. *Numer. Math.* **2003**, *94*, 33–65. [[CrossRef](#)]
- Wheeler, A.A.; Boettinger, W.J.; Mcfadden, G.B. Phase-field model for isothermal phase transitions in binary alloys. *Phys. Rev. A* **1992**, *45*, 7424–7439. [[CrossRef](#)] [[PubMed](#)]
- Sabir, M.; Shah, A.; Muhammad, W.; Ali, I.; Bastian, P. A mathematical model of tumor hypoxia targeting in cancer treatment and its numerical simulation. *Comput. Math. Appl.* **2017**, *74*, 3250–3259. [[CrossRef](#)]
- Kolobov, A.V.; Gubernov, V.V.; Polezhaev, A.A. Autowaves in a model of invasive tumor growth. *Biophysics* **2009**, *54*, 232–237. [[CrossRef](#)]
- Avila, J.A.; Lozada-Cruz, G. On a model for the growth of an invasive avascular tumor. *Appl. Math. Inf. Sci.* **2013**, *7*, 1857–1863. [[CrossRef](#)]
- Zahra, W.K. Trigonometric B-Spline collocation method for solving PHI-Four and Allen-Cahn equations. *Mediterr J. Math.* **2017**, *14*, 122–141. [[CrossRef](#)]
- Karasözen, B.; Uzunca, M.; Sariaydin-Filibelioglu, A.; Yücel, H. Energy stable discontinuous Galerkin finite element method for the Allen-Cahn equation. *Int. J. Comp. Methods* **2018**, *15*, 1850013. [[CrossRef](#)]
- Yang, J.; Du, Q.; Zhang, W. Uniform L^p -bound of the Allen-Cahn equation and its numerical discretization. *Int. J. Numer. Anal. Model.* **2018**, *15*, 213–227.
- Liu, C.-S.; Kuo, C.-L. A multiple-scale Pascal polynomial triangle solving elliptic equations and inverse Cauchy problems. *Eng. Anal. Bound. Elem.* **2016**, *62*, 35–43. [[CrossRef](#)]
- Liu, C.-S.; Young, D.-L. A multiple-scale Pascal polynomial for 2D Stokes and inverse Cauchy-Stokes problems. *J. Comput. Phys.* **2016**, *312*, 1–13. [[CrossRef](#)]
- Chang, C.-W. A new meshless method for solving steady-state nonlinear heat conduction problems in arbitrary plane domain. *Eng. Anal. Bound. Elem.* **2016**, *70*, 56–71. [[CrossRef](#)]
- Chang, C.-W.; Huang, J.-H.; Wang, C.-C. A new meshfree method for solving steady-state modified Burgers' equation in transport problems. *Smart Sci.* **2017**, *5*, 14–20. [[CrossRef](#)]

